R-modes of accreting hyperon stars as persistent sources of gravitational waves

Mohit Nayyar and Benjamin J. Owen
Institute for Gravitational Physics and Geometry and Center for Gravitational Wave Physics, Department of Physics, The Pennsylvania State University, University Park, PA 16802-6300
(Dated: Id: paper.tex,v 1.92 2006/03/22 04:46:31 nayyar Exp)

The r-modes of accreting neutron stars could be a detectable source of persistent gravitational waves if the bulk viscosity of the stellar matter can prevent a thermal runaway. This is possible if exotic particles such as hyperons are present in the core of the star. We compute bulk viscous damping rates and critical frequencies for r-modes of neutron stars containing hyperons in the framework of relativistic mean field theory. We combine the results of several previous calculations of the microphysics, include for the first time the effect of rotation, and explore the effects of various parameters on the viability of persistent gravitational wave emission. We find that persistent emission is quite robust, although it is disfavored in stars below 1.3–1.5 $M_\odot$ depending on the equation of state. In some cases persistent emission is compatible with temperatures as low as 10^7 K, observed in some accreting neutron stars in quiescence.

PACS numbers: 04.30.Db, 04.40.Dg, 26.60.+c, 97.10.Sj

I. INTRODUCTION

The r-modes (fluid oscillations governed by the Coriolis force) of rapidly rotating neutron stars have attracted much interest as possible sources of gravitational waves and mechanisms for regulating the spins of neutron stars. See Ref. [1] for a recent review of the many physical and astrophysical issues related to the r-modes; here we focus on gravitational wave emission. Gravitational radiation drives the r-modes unstable and could lead to detectable gravitational wave emission in two scenarios. In one scenario, a newborn neutron star could radiate a substantial fraction of its rotational energy and angular momentum as gravitational waves changing in frequency on a timescale of a year or more [2]. In the other scenario, r-modes in rapidly accreting neutron stars in low-mass x-ray binaries (LMXBs) could be persistent sources of periodic gravitational waves [3, 4]. (Here the r-modes provide a specific mechanism for a more general torque balance argument [5, 6]).

Currently the latter scenario for gravitational wave emission (from LMXBs) looks like a brighter prospect for detection. There is now evidence from several approaches that the amplitude of an r-mode growing due to the instability is limited by nonlinear fluid dynamics to a relatively small value [7, 8, 9, 10, 11, 12, 13]. While low-amplitude long-lived r-modes in newborn neutron stars still can lead to astrophysically interesting effects such as the regulation of spins, a low mode amplitude renders the gravitational wave signal undetectable unless there is a very nearby supernova [2]. Also, if neutron stars contain particles more exotic than neutrons and protons—such as hyperons, where an up or down quark in a nucleon is replaced by a strange quark—there are additional viscous damping mechanisms which may eliminate the instability altogether in very young, hot neutron stars [14, 15, 16, 17, 18, 19, 20, 21] or strange quark stars [22]. However, for the LMXB scenario, low amplitude is not a problem [3, 4] and the additional viscosity actually renders stars with exotic particles better candidates for gravitational wave detection. The reason for the latter is subtle, and bears explanation.

Real neutron stars are not perfect fluids, and thus viscous (and other) damping mechanisms compete with gravitational wave driving of the r-modes. The strengths of the driving and damping mechanisms can be expressed as timescales which depend on the rotation frequency and temperature of the star (usually assumed to be nearly isothermal). Therefore it is useful to consider the location of a star in the temperature-frequency plane, as shown in Fig. 1. The strength of viscosity can be graphically represented by a curve in that plane that is the locus of all points where the driving and damping timescales are equal—this defines a critical frequency as a function of temperature. Since the driving timescale decreases with frequency, stars above the critical frequency curve have one or more unstable r-modes, while stars below it are stable and stars on it are marginally stable.

Figure 1 plots examples of critical frequency curves in the temperature range 10^8 K$\ll T \ll 10^{10}$ K appropriate for the LMXB emission scenario. (The needed range is higher than most observed temperatures of LMXBs in quiescence because of a thermal runaway; see below.) At low temperatures the damping in Fig. 1 is taken to be dominated by shear viscosity in a boundary layer between the solid crust and fluid core (from Ref. [23], augmented by a constant relative crust-core velocity in the range discussed in Ref. [24]). There are many other possible curves for the low temperature part of the plot, corresponding to more complicated damping mechanisms such as turbulence [25] or superfluid magnetoviscous effects [26], but they generally share the qualitative property of decreasing with temperature. (Some low-temperature curves lie above the observed range of spins entirely, but the observed spins of low-mass x-ray binaries are easier to explain if the curve lies in the region indicated [3, 4, 27].) At high temperatures the damping is probably dominated by bulk viscosity, either from the Urca process (pertur-

bation of β-equilibrium) or from nonleptonic processes involving strange particles such as hyperons. The Urca process, which requires no exotic particles, does not affect the critical frequency curve for $T < 10^{10}$ K and thus does not show up in Fig. 1. Thus the top plot in Fig. 1 shows a critical frequency curve for a neutron star, and the bottom plot shows such a curve for a star with hyperons (with the high-temperature part of the curve derived from Ref. [19]). This type of plot looks encouraging for gravitational wave detection because there is plenty of room above the curve for stars to be unstable and thus emitting gravitational waves.

However, the gravitational wave emission duty cycle could be much smaller than 100% due to a thermal runaway [28, 29]. This happens generically when the critical frequency decreases with temperature. In that case, plotted at the top of Fig. 1, a star will execute a loop as shown and radiate only during the time it spends above the curve. A stable star which begins at the bottom left of the loop is spun up by accretion until it moves above the critical frequency and the instability is triggered. The shear from the growing r-modes then causes the star to heat up, moving it rightwards on the loop. As the temperature rises, so does the rate of neutrino cooling, causing the star to drop down toward the critical frequency again at a temperature of a few times 10^9 K. After falling below the critical frequency, the r-mode heating is removed and the star drifts leftward along the bottom of the loop until returning to its initial position. Although the time it takes for a star to complete the loop is dominated by the accretion rate, the timescale for gravitational wave emission depends mainly on the saturation amplitude of r-mode oscillations. For a saturation amplitude (α in the notation of Ref. [30]) of order unity, the duty cycle for gravitational wave emission is of the order 10^{-6} [28]. Whereas the duty cycle can be as high as about 30% for the lowest predicted values of the saturation amplitude ($\alpha \simeq 10^{-5}$), for typical estimates of the saturation amplitude ($\alpha \simeq 10^{-4}$) the duty cycle is only of order 10^{-1} [31]. Advanced LIGO will be able to detect at most one LMXB (Sco X-1) without narrowbanding (and hurting its ability to see other sources), or 6–7 LMXBs with narrowbanding around a series of different frequencies [32]. The small number of detectable systems and the fact that the timescale for a star to complete a loop is much longer than a human lifetime mean that a duty cycle of order 10^{-1} or less is pessimistic for gravitational wave searches for the r-modes.

If the critical frequency increases with temperature as in the bottom plot of Fig. 1, the thermal runaway can be blocked. A rapidly accreting star in an LMXB can have a duty cycle of order unity for emission of gravitational radiation as it sits on the curve or makes small peregrinations about it [33]. (It could also keep emitting, although less detectably, for some time after the rapid accretion shuts off [34].) This could happen for stars which exhibit a rise in the critical frequency curve at a low enough temperature. The rise is typical for stars where

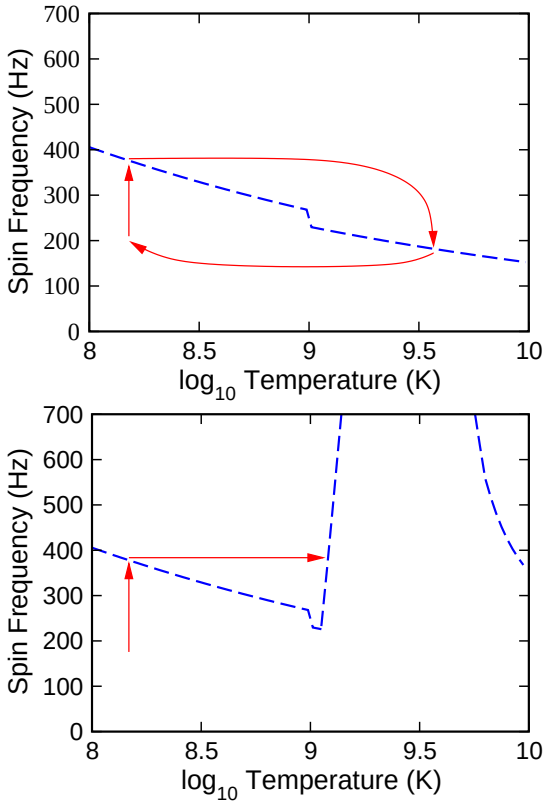

FIG. 1: Critical frequency curves are given (qualitatively) by the dashed lines. The top plot includes no bulk viscosity due to hyperons or other strange particles. In this case an accreting neutron star traversing the loop indicated undergoes a thermal runaway and has a low gravitational radiation duty cycle. The bottom plot includes hyperon bulk viscosity. In this case the thermal runaway is blocked, and an accreting star is a source of persistent gravitational waves as it remains in equilibrium at the last arrowhead.

high bulk viscosity processes involving hyperons [35, 36] or strange quarks [37] are at work. Thus the case for the gravitational wave emission scenario is in fact strengthened by high bulk viscosity from processes which are fundamentally quark-quark interactions. One might expect similar critical frequency curves to arise for stars containing other forms of strange matter such as a kaon condensate or mixed quark-baryon phase, but this has yet to be investigated. The thermal runaway is blocked if the increase in temperature (width of the loop in Fig. 1) is enough to take the star from the negatively sloped part of the instability curve to the positively sloped part. The larger the saturation amplitude of r-modes the greater is the increase in the temperature. Whether the star makes the jump to the positively sloped curve also depends on which cooling mechanisms are operative, and on the shape of the low-temperature instability curve, which in turn depends on which damping mechanism dominates at low temperatures. Notwithstanding the wide range of estimates for α, the shape of the negatively sloped curve, and the cooling mechanisms, the question of the r-modes

in LMXBs as a persistent source of gravitational radiation comes down to asking whether there is a rise in the instability curve around 10^9 K or lower.

Our purpose in this paper is to revisit the question of whether there is a rise in the critical frequency curve around 10^9 K or lower, as in the bottom of Fig. 1, leading to persistent gravitational wave emission. We focus (for now) on neutron stars containing hyperons (hyperon stars), because hyperons are in some sense the most conservative and robust of the many proposals for exotic matter in the cores of neutron stars: Some properties of hyperons can be measured in the laboratory, both in vacuum and in the environment of a light nucleus, which combined with astronomical observations allows one to constrain some of the many uncertainties in building an equation of state [38, 39]. Equations of state which allow for hyperons generally produce them at densities relevant for neutron stars, about twice nuclear density and up.

We synthesize and extend results of previous work on this topic. In arguing the case for persistent gravitational wave emission, Wagoner [35, 36] and Reisenegger and Bonacic [34] base their critical frequency curves on bulk viscosity coefficients obtained by combining the results of Lindblom and Owen [19] (hereafter LO) and Haensel, Levenfish, and Yakovlev [20] (hereafter HLY). The LO and HLY viscosities were obtained by different calculations and produced somewhat different results. LO used a detailed self-consistent model of a multicomponent fluid described by relativistic mean field theory [38], but since they were primarily concerned with the high-temperature regime appropriate to newborn neutron stars they treated the effect of superfluidity with a rough approximation. LO also made some errors which resulted in a bulk viscosity coefficient a factor of 20 or more too high. HLY were more careful with superfluidity, using consistent damping factors in the collision integrals, but instead of evaluating reaction rates and thermodynamic derivatives within relativistic mean field theory they used "order of magnitude estimates" of some quantities which resulted in more than an order of magnitude disagreement with the microscopic results of LO (and with Jones [18]). We correct some mistakes in LO and combine their self-consistent microphysical model with a more careful treatment of superfluidity similar to that of HLY. We also treat the macroscopic physics more carefully than LO, including the effect of rotation on stellar structure which in some cases can significantly affect damping timescales and critical frequency curves. (HLY made only order of magnitude estimates of mode damping timescales and did not plot critical frequency curves.)

We also address the question "Does the viability of persistent gravitational wave emission require fine tuning of parameters?" Many of the parameters that go into building the equation of state have significant uncertainties, and those that go into computing reaction rates and bulk viscosities are even more uncertain. We investigate the viability of persistent gravitational wave emission with respect to variation of several microphysical numbers such as hyperon coupling constants and the superfluid bandgap, and even which nonleptonic reaction is most important (taking into account the results of van Dalen and Dieperink [21]). We also investigate the dependence on the mass of the star, since cooling observations [40] and timing of radio pulsars in binaries [41, 42] indicate a wider mass range than the traditionally assumed clustering around 1.4 $M_\odot$. (Cooling observations also might be interpreted to favor the existence of strange particles such as hyperons, although the data still can be fit by exotic cooling from purely nucleonic matter.)

The organization of the rest of the paper is as follows. In Sec. II we describe the microphysical model which leads to the equation of state and ultimately the macroscopic coefficient of bulk viscosity. In Sec. III we plot the critical frequency curves for a range of neutron star masses and microphysical parameters. In Sec. IV we summarize our findings and discuss possible improvements.

II. MICROPHYSICS

We model the composition of a neutron star within the framework of relativistic mean field theory industrialized by Glendenning and described in Ref. [38]. Here we do not consider meson condensates or exotica such as a mixed quark-baryon phase, but do allow for the presence of hyperons which are somewhat constrained by laboratory and astronomical data.

A. Equation of state

There are several free parameters in this framework, some of which are better known than others. We use a range of parameters set by combining the old laboratory constraints with recent astronomical observations [39]. At nuclear density (2–3$\times 10^{15}$ g/cm^3) the matter is, as in all models, composed of neutrons, protons, electrons, and muons. As the density rises hyperons generically appear, their order of appearance (and density thresholds) changing somewhat with the precise set of parameter values but roughly corresponding to Σ^-, Λ, Σ^0, Σ^+, Ξ^-, starting at roughly twice nuclear density. Other baryons typically appear in this framework only at densities higher than those found in the cores of the most massive neutron stars, nearly 10 times nuclear density. At such high densities the asymptotic freedom of the strong nuclear force is likely to lead to quark matter anyway, and any baryonic model must be considered somewhat suspect. As we shall see, most of the astrophysically important dissipation comes from lower densities (2–3 times nuclear density) where this deficiency of the model is not important, i.e. low-energy effective field theory is good enough. The framework of relativistic mean field theory has some advantages over others, such as an inherently causal equation of state even at high densities, but has

some disadvantages including the neglect of correlations between particles which should become more important at high densities.

In this framework, the strong interaction between baryons is modeled as a tree-level exchange of isoscalar mesons σ, vector mesons ω, and isovector mesons ρ. The effective Lagrangian includes kinetic and tree-level interaction terms for the baryons, leptons, and mesons, as well as an effective potential for the σ expanded up to $O(\sigma^4)$. The variables of the theory are the Fermi momenta k_i of the baryons and leptons, supplemented by the field strengths of the σ, ω, and ρ mesons. Expansion coefficients and coupling constants can be fit to numbers extracted from measurements of nuclei and hypernuclei at saturation density. The fitting process (and Lagrangian) is described in detail in Ref. [38]. We use an updated set of fit parameters from Ref. [39].

For N species of baryons, two of leptons, and three of mesons, the composition of the matter consists of $N+5$ unknowns (the baryon, lepton and meson fields) which must be determined by $N+5$ equations. The first three equations are the Euler-Lagrange equations for the mesons determined by varying the effective Lagrangian of Ref. [38]. The equations are rendered tractable by assuming that the fields are given by their mean values in a uniform static ground state, and take the form

$$\omega_0 = \sum_B \frac{g_{\omega B}}{m_\omega^2} n_B, \tag{1}$$

$$\rho_{03} = \sum_B \frac{g_{\rho B}}{m_\rho^2} I_{3B} n_B, \tag{2}$$

$$m_\sigma^2 \sigma = \sum_B g_{\sigma B} \rho_{s,B} - b m_N g_\sigma (g_\sigma \sigma)^2 - c g_\sigma (g_\sigma \sigma)^3. \tag{3}$$

Here the index B labels baryon species, ω_0 is the timelike component of the vector meson field (the spatial components vanish), n_B is the number density of baryon B, and ρ_{03} is the isospin 3-component of the timelike component of the isovector meson field. Throughout this Section we use units such that $\hbar = c = 1$. The scalar density is given by

$$\rho_{s,B} = \sum_B \frac{2J_B+1}{2\pi^2} \int_0^{k_B} \frac{m_B^{\star 2}(\sigma)}{\sqrt{k^2 + m_B^{\star 2}(\sigma)}} k^2 dk. \tag{4}$$

The coupling constants between the baryon B and the mesons are given by $g_{\sigma B}$, $g_{\omega B}$, and $g_{\rho B}$. We assume, as in Ref. [38], that they are given by one set of values $(g_\sigma, g_\omega, g_\rho)$ for the nucleons and another $(x_\sigma g_\sigma, x_\omega g_\omega, x_\rho g_\rho)$ for the hyperons, so that the x's measure relative coupling strengths for hyperons. The coupling constants for the self-interaction terms of the scalar field are b and c. The masses of the mesons are given by m_σ, m_ω, and m_ρ. The quantities for the Bth baryon I_{3B} and J_B are, respectively, its 3-component of isospin, and its spin. The Fermi momentum of the baryon species is given by k_B while its effective mass is given by $m_B^* = m_B - g_{\sigma B}\sigma$. The quantity m_N represents the average mass of a nucleon and is used to make b and c dimensionless. The constraints of charge neutrality and conservation of baryon number (if a particular baryon number density n is assumed) provide two more equations which can be written, respectively, as

$$\sum_i n_i q_i = 0, \tag{5}$$

$$\sum_B n_B = n. \tag{6}$$

Here n_i denotes the number density of fermion species i and q_i is its electric charge in units of e. Now we are down to N unknowns, which can be eliminated with the N equations of generalized β-equilibrium

$$\mu_i = b_i \mu_n - q_i \mu_e. \tag{7}$$

(The neutrinos are assumed to have zero chemical potential.) Here μ_i is the chemical potential of fermion species i and b_i is its baryon charge. (Actually there are $N+2$ equations of β-equilibrium including the leptons, but the equations for the electron and neutron are identities and thus do not count toward the elimination of unknowns.) The chemical potential of each baryon species is given by

$$\mu_B = g_{\omega B}\omega_0 + g_{\rho B}\rho_{03} I_{3B} + \sqrt{k_B^2 + m_B^{*2}}, \tag{8}$$

while that of each lepton species is given by

$$\mu_L = \sqrt{k_L^2 + m_L^2}. \tag{9}$$

Here k_L and m_L are, respectively, the Fermi momentum and mass of the Lth leptonic species.

For a given baryon number density n, the baryon, meson, and lepton fields are found by simultaneously solving Eqs. (1)–(7). The numerical technique is based on a multi-dimensional root finder and thus requires an initial guess to ensure finding the correct root. We first solve for a low value n below saturation density where the system can be approximated as a weakly interacting Fermi gas and analytic approximations can be found as in Ref. [38]. The code then steps up in baryon density n, at each step using the previous step's values for the unknowns as the initial guess for the root finder. Once the fields are found for a given n, the mass-energy density ϵ and pressure p can be determined:

$$\begin{aligned}
\epsilon &= \frac{1}{3} b m_N (g_\sigma \sigma)^3 + \frac{1}{4} c (g_\sigma \sigma)^4 + \frac{1}{2} m_\sigma^2 \sigma^2 \\
&\quad + \frac{1}{2} m_\omega^2 \omega_0^2 + \frac{1}{2} m_\rho^2 \rho_{03}^2 \\
&\quad + \sum_B \frac{1}{\pi^2} \int_0^{k_B} \sqrt{k^2 + m_B^{*2}}\, k^2 dk \\
&\quad + \sum_L \frac{1}{\pi^2} \int_0^{k_L} \sqrt{k^2 + m_L^2}\, k^2 dk,
\end{aligned} \tag{10}$$

$$p = -\frac{1}{3} b m_N (g_\sigma \sigma)^3 - \frac{1}{4} c (g_\sigma \sigma)^4 - \frac{1}{2} m_\sigma^2 \sigma^2$$

TABLE I: Parameters for five relativistic mean field equations of state used in this paper.

Name	K (MeV)	m^*/m_N	x_σ
H3	300	0.70	0.60
H4	300	0.70	0.72
H5	300	0.80	0.66
H6	240	0.70	0.67
H7	240	0.80	0.68

$$+\frac{1}{2}m_\omega^2\omega_0^2+\frac{1}{2}m_\rho^2\rho_{03}^2 +\sum_B\frac{1}{\pi^2}\int_0^{k_B}\frac{k^4dk}{\sqrt{k^2+m_B^{*2}}} +\sum_L\frac{1}{\pi^2}\int_0^{k_L}\frac{k^4dk}{\sqrt{k^2+m_L^2}}. \quad (11)$$

Here the summations are over the baryon species (B) and the lepton species (L). These expressions can be combined to produce tabulations of $p(\epsilon)$, the equation of state.

There remains the problem of choosing the values of the constants $(g_\sigma/m_\sigma)^2$, $(g_\omega/m_\omega)^2$, $(g_\rho/m_\rho)^2$, b, c, x_σ, x_ω, and x_ρ. Each choice of constants produces a different equation of state with different hyperon threshold densities, neutron star maximum mass, etc. We use five equations of state from [39] chosen to be compatible with recent measurements of neutron star masses [41, 42] and a gravitational redshift [43] as well as hypernuclear data [38]. The constants in Eqs. (1)–(7) are fit in the manner of Glendenning [38] to a Λ binding of -28 MeV, saturation density 0.153 fm^{-3}, binding energy per nucleon -16.3 MeV at saturation, and isospin asymmetry coefficient 32.5 MeV, as well as a range of incompressibilities K, nucleon effective masses m^*, and hyperon couplings x_σ. Since it is easiest to qualitatively understand the equations of state in terms of the latter three parameters, we give them in Table I. Low K and high m^* lead to a soft equation of state, while high K and low m^* lead to a stiff equation of state. Since most of the matter in the star is at high density, the hard core repulsion dominates the strong interaction. Thus high x_σ postpones hyperon formation to higher densities, reducing hyperon populations (and thus viscosity) and stiffening the equation of state.

All of these equations of state are somewhat different from that used by LO and HLY. Though both HLY and LO use the "case 2" equation of state from an older paper by Glendenning [44], there were misprints in that paper which were corrected by HLY but not by LO. The scalar self interaction coupling constants b and c in Ref. [44] should be 3 and 4 times larger, respectively, than the values that are quoted for them. Also, case 2 of Ref. [44] used $K = 285$ MeV and $x_\sigma = x_\omega = x_\rho = \sqrt{2/3}$, and had several minor differences in other constants (we use values from the 2002 Particle Data Group review [45]). As a result, the newer equations of state we use have higher hyperon populations and thus higher viscosities.

B. Relaxation timescale

The reactions that contribute most to bulk viscosity are the weak interaction processes, as their relaxation timescales are within a few orders of magnitude of the r-mode period (milliseconds).

Among these, the most significant that can be calculated from first principles are the non-leptonic weak interactions involving the lightest hyperons, Σ^- and Λ, as they occur at lower densities than the more massive particles and thus have higher populations in a given star. Following LO, we calculate matrix elements for the reactions

$$n+n \leftrightarrow p+\Sigma^- \quad (12)$$
$$n+p \leftrightarrow p+\Lambda \quad (13)$$

as tree-level Feynman diagrams involving the exchange of a W boson. The latter reaction was also considered (with a phenomenological free parameters) by HLY. These reactions are combined to calculate an overall microscopic relaxation timescale. (This is the timescale on which a small perturbation of the neutron fraction returns to its equilibrium value.)

In addition to these reactions, Jones [18] includes

$$n+n \leftrightarrow n+\Lambda \quad (14)$$

which is the dominant nonleptonic process observed in Λ hypernuclei in the laboratory. We do not consider this reaction as it has no contribution based on a W-boson exchange, even though the bare-mass interaction rate for this process is known. Using Eq. (15) from Jones [18] we estimate that reaction (14) has a relaxation timescale that is longer than the timescale of the Λ reaction (13) by a factor of about 2 and thus does not change the final viscosity much. (When accounting for the macroscopic structure of the star, the Σ^- process dominates the overall bulk viscosity since the Σ^- population extends to lower densities and therefore a greater volume fraction of the star than the Λ population.) There are various other concurrently occuring processes which contribute to the net reaction rate but their rates are not easy to predict. Even these rates are subject to substantial uncertainties: Van Dalen and Dieperink [21] use a meson-exchange model for all three hyperon reactions and find reaction rates of order 10–100 times greater than LO and thus bulk viscosity coefficients 10–100 times lower than LO. (As we shall see in the next section, such a change has less of an effect on the r-mode critical frequency than one might think.) Our result for the net rate is then a lower limit, and consequently an upper limit on the bulk viscosity, in the typical range of temperatures for LMXBs.

To summarize the results of LO, the relaxation timescale can be computed as a function of the equilibrium matter fields. Neglecting superfluidity, the result is

$$\frac{1}{\tau} = \frac{(kT)^2}{192\pi^3} k_\Sigma \langle|\mathcal{M}_\Sigma^2|\rangle \frac{\delta\mu}{n\, x_n} \tag{15}$$

when the Λ hyperons have not yet appeared and

$$\frac{1}{\tau} = \frac{(kT)^2}{192\pi^3} \left(k_\Sigma \langle|\mathcal{M}_\Sigma^2|\rangle + k_\Lambda \langle|\mathcal{M}_\Lambda^2|\rangle\right) \frac{\delta\mu}{n\, x_n} \tag{16}$$

when both Λ and Σ^- are present. Here kT is Boltzmann's constant times the temperature. The matrix elements $\mathcal{M}$ are computed as tree-level Feynman diagrams, squared, summed over initial spinors, and averaged over the angular part of the collision integral (indicated by $\langle\rangle$). (Note that van Dalen and Dieperink [21] do not angle average.) They are functions of the Fermi momenta and meson fields given by Eqs. (4.28) and (4.29) of LO,

$$\begin{aligned}
\langle|\mathcal{M}_\Lambda|^2\rangle \;=\; & \frac{G_F^2 \sin^2 2\theta_C}{15} \left\{120\left(1-g_{np}^2\right)\left(1-g_{p\Lambda}^2\right) m_n^* m_p^{*2} m_\Lambda^* - 20\left(1-g_{np}^2\right)\left(1+g_{p\Lambda}^2\right) m_n^* m_p^* \left(3\mu_p\mu_\Lambda - k_\Lambda^2\right)\right. \\
& -10\left(1+g_{np}^2\right)\left(1-g_{p\Lambda}^2\right) m_p^* m_\Lambda^* \left(6\mu_n\mu_p - 3k_n^2 + k_\Lambda^2\right) + 2\left[\left(1+g_{np}^2\right)\left(1+g_{p\Lambda}^2\right) + 4g_{np}g_{p\Lambda}\right] \\
& \times \left[5\mu_p\mu_\Lambda\left(6\mu_n\mu_p + 3k_n^2 - k_\Lambda^2\right) + k_\Lambda^2\left(10\mu_n\mu_p + 5k_n^2 + 10k_p^2 - k_\Lambda^2\right)\right] + \left[\left(1+g_{np}^2\right)\left(1+g_{p\Lambda}^2\right) - 4g_{np}g_{p\Lambda}\right] \\
& \left.\times \left[10\mu_n\mu_\Lambda\left(6m_p^{*2} + 3k_n^2 + k_\Lambda^2\right) + k_\Lambda^2\left(-20\mu_p^2 + 15k_p^2 - 3k_\Lambda^2 + 5(k_n^2 - k_p^2)^2/(k_p^2 - k_\Lambda^2)\right)\right]\right\}, \qquad (17) \\
\langle|\mathcal{M}_\Sigma|^2\rangle \;=\; & \frac{2}{15} G_F^2 \sin^2 2\theta_C \left\{180\left(1-g_{np}^2\right)\left(1-g_{n\Sigma}^2\right) m_n^{*2} m_p^* m_\Sigma^* - 40\left(1-g_{np}^2\right)\left(1+g_{n\Sigma}^2\right) m_n^* m_p^* \left(3\mu_n\mu_\Sigma - k_\Sigma^2\right) - 20\right. \\
& \times \left(1+g_{np}^2\right)\left(1-g_{n\Sigma}^2\right) m_n^* m_\Sigma^* \left(6\mu_n\mu_p - 3k_p^2 + k_\Sigma^2\right) - 5\left(1-g_{np}^2\right)\left(1-g_{n\Sigma}^2\right) m_p^* m_\Sigma^* \left(6\mu_n^2 + 6k_n^2 - 3k_p^2 - k_\Sigma^2\right) \\
& +4\left[\left(1+g_{np}^2\right)\left(1+g_{n\Sigma}^2\right) + 4g_{np}g_{n\Sigma}\right]\left[10\mu_n^2\left(3\mu_p\mu_\Sigma + k_\Sigma^2\right) + 5\mu_p\mu_\Sigma\left(6k_n^2 - 3k_p^2 - k_\Sigma^2\right) + k_\Sigma^2\left(10k_n^2 + 5k_p^2\right.\right. \\
& \left.\left.-k_\Sigma^2\right)\right] + \left[\left(1+g_{np}^2\right)\left(1+g_{n\Sigma}^2\right) - 4g_{np}g_{n\Sigma}\right]\left[-10m_n^{*2}\left(3\mu_p\mu_\Sigma + k_\Sigma^2\right) + 10\mu_n\left(6\mu_n\mu_p\mu_\Sigma - 2\mu_p k_\Sigma^2 - 3\mu_\Sigma k_p^2\right.\right. \\
& \left.\left.\left.+\mu_\Sigma k_\Sigma^2\right) + 15k_p^2 k_\Sigma^2 - 3k_\Sigma^4\right]\right\}. \qquad (18)
\end{aligned}$$

We reproduce them here since the latter equation in LO is missing some terms (although the code used to generate the LO results is not missing them). Also, LO actually used kinetic energies instead of chemical potentials which should be used to be consistent with the quasiparticle picture of Fermi liquid theory. Correcting this reduces the relaxation time by a factor of 10 or more, making up much of the difference with the results of van Dalen and Dieperink [21] who use a drastically different model of the interaction. In the matrix elements, G_F is the Fermi constant and θ_C is the Cabibbo angle. The g's are axial-vector coupling constants, which we take to have their values measured from vacuum β-decay of particles at rest [45]. The remaining factor on the far right of Eqs. (15) and (16) is explained in the next subsection.

HLY, in contrast, used the nonrelativistic limit

$$\langle|\mathcal{M}_\Sigma|^2\rangle = 4G_F^2 \sin^2 2\theta_C \left(1 + 3g_{np}g_{n\Sigma}\right)^2 \tag{19}$$

of Eq. (18) and left the term in parentheses as a phenomenological parameter, which they simply set to 0.1. This is somewhat justified because the Particle Data group values for the couplings g_{np} and $g_{n\Sigma}$ result in a near-perfect cancellation of the term. Any in-medium change of these values would have a disproportionately large effect as a result. We (and LO) find that including the full Eq. (18) erases the effect of the near-cancellation of the leading-order terms and produces a running value of the term which can increase by more than an order of magnitude above 0.1.

C. Bulk viscosity

We use for ζ, the macroscopic coefficient of bulk viscosity, the special relativistic expression derived by Lindblom and Owen [19]:

$$\zeta = \frac{p(\gamma_\infty - \gamma_0)\tau}{1 + (\hat{\omega}\tau)^2}. \tag{20}$$

where p is the pressure, $\hat{\omega}$ is the angular frequency of the r-mode in a frame corotating with the star, and τ is the net microscopic relaxation time we just computed. The fast adiabatic index γ_∞ (for infinite-frequency perturbations) can be written as

$$\gamma_\infty = \sum_i \frac{n_i}{n}\left(\frac{\partial p}{\partial n_i}\right), \tag{21}$$

where $n_i = k_i^3/(3\pi^2)$ is the number density of species i and the partial derivatives can be evaluated explicitly from Eq. (11). The slow adiabatic index γ_0 (for zero-

frequency perturbations) can be written as

$$\gamma_0 = \left(\frac{n}{p}\right)\left(\frac{dp}{dn}\right), \tag{22}$$

and is straightforward to evaluate for example by differentiating the equation of state. However, while LO derived the correct relativistic expression and noted that it reduces the factor $\gamma_\infty - \gamma_0$ by a factor of 2–2.5 from the nonrelativistic expression, their Fig. 2 and code for the rest of the paper incorrectly used a data file with the nonrelativistic expression and thus are a factor 2–2.5 too high.

Now we address the factor $\delta\mu/\delta x_n$ in Eqs. (15) and (16) in the same manner as LO. This factor is determined by the constraints of charge and baryon conservation (5) and (6), plus the constraint that the reaction

$$n + \Lambda \leftrightarrow p^+ + \Sigma^- \tag{23}$$

is in equilibrium since its reaction rate is many orders of magnitude greater than the weak interaction rates. This implies that both the non-leptonic reactions have the same chemical potential imbalance:

$$\delta\mu \equiv \delta\mu_n - \delta\mu_\Lambda = 2\delta\mu_n - \delta\mu_p - \delta\mu_\Sigma. \tag{24}$$

Assuming small perturbations and using the neutron fraction x_n, this yields the relation

$$\begin{aligned}\frac{\delta\mu}{n_B\delta x_n} &= \alpha_{nn} + \frac{(\beta_n-\beta_\Lambda)(\alpha_{np}-\alpha_{\Lambda p}+\alpha_{n\Sigma}-\alpha_{\Lambda\Sigma})}{2\beta_\Lambda-\beta_p-\beta_\Sigma} \\ &\quad -\alpha_{\Lambda n} - \frac{(2\beta_n-\beta_p-\beta_\Sigma)(\alpha_{n\Lambda}-\alpha_{\Lambda\Lambda})}{2\beta_\Lambda-\beta_p-\beta_\Sigma},\end{aligned} \tag{25}$$

where β_i is given by

$$\beta_i = \alpha_{ni} + \alpha_{\Lambda i} - \alpha_{pi} - \alpha_{\Sigma i}. \tag{26}$$

and α_i is given by

$$\alpha_{ij} = \left(\frac{\partial\mu_i}{\partial n_j}\right)_{n_k, k\neq j}. \tag{27}$$

These expressions apply for densities where the Λ and Σ^- hyperons are both present. In the regime where only the Σ^- hyperon is present the strong interaction constraint is no longer a factor and one obtains a simpler form

$$\begin{aligned}\frac{2\delta\mu}{n_B\delta x_n} &= 4\alpha_{nn} - 2(\alpha_{pn}+\alpha_{\Sigma n}+\alpha_{np}+\alpha_{n\Sigma}) \\ &\quad +\alpha_{pp}+\alpha_{\Sigma p}+\alpha_{p\Sigma}+\alpha_{\Sigma\Sigma}.\end{aligned} \tag{28}$$

LO used numerical differencing to calculate the derivatives α_{ij}, but due to a coding error the σ meson field was not differenced properly. The maximum error this induces in the value of $\delta\mu/n_B\delta x_n$ is less than 0.3%, well below the uncertainties of the problem.

D. Superfluidity

In the temperature range of interest (below 10^{10} K), nucleons and hyperons are expected to form Cooper pairs near their Fermi surfaces and act as superfluids. This greatly slows reaction rates and has an important effect on transport coefficients such as bulk viscosity.

The energy associated with the Cooper pairing is given by the bandgap. Assuming ${}^1S_0$ pairing, the zero-temperature bandgap Δ_0 is related to the superfluid critical temperature T_C by [46]

$$kT_C = 0.57\Delta_0. \tag{29}$$

We use the LO fit to the finite-temperature bandgap

$$\Delta(T) = \Delta_0\left[1 - \left(\frac{T}{T_C}\right)^{3.4}\right]^{0.53}. \tag{30}$$

For the Λ hyperons we use the empirical fit made by LO to the zero-temperature gap function $\Delta_{0\Lambda}$ of the Λ hyperon as computed by Balberg and Barnea [47]. The calculation by Balberg and Barnea [47] is constrained by experiments on double Λ hypernuclei, though like other calculations of Δ_Λ it is likely only good to within a factor of 2 or 3. The zero-temperature gap depends on the total baryon number density n and on the Fermi momentum k_Λ in a way that LO found was well fit by

$$\begin{aligned}\Delta_{0\Lambda}(k_\Lambda, n) &= 5.1{k_\Lambda}^3(1.52-k_\Lambda)^3 \\ &\quad \times\left[0.77 + 0.043\,(6.2n-0.88)^2\right].\end{aligned} \tag{31}$$

Here $\Delta_{0\Lambda}$ is in MeV, k_Λ in fm^{-1}, and n in fm^{-3}. Thus the critical temperature for Λ superfluidity peaks somewhat below 10^{10} K.

The Σ^- superfluid bandgaps are not as well known as Δ_Λ due to the absence of similar experiments on hypernuclei containing the Σ^- hyperon. Determination of the hypernuclei energy levels for the Σ^- hyperon are constrained by the very short decay time of the hyperon. Takatsuka et al [48] have however calculated, using several models of the nuclear interaction, that the bandgap lies in the range $\Delta_\Lambda \leq \Delta_{\Sigma^-} \leq 10\Delta_\Lambda$. To account for the uncertainty in the bandgap we perform our calculation for two cases as in LO: when $\Delta_{\Sigma^-} = \Delta_\Lambda$ and when $\Delta_{\Sigma^-} = 10\Delta_\Lambda$.

For the superfluidity of protons we use model 2p of Ref. [49], which is one of the bandgap models used by HLY. (LO did not model proton superfluidity, since it was not relevant at the temperatures greater than 10^{10} K that they considered.) This bandgap model is not based on a specific calculation of the bandgap but preserves the general features of bandgaps predicted by various microscopic theories. In this model the zero temperature gap depends only on the Fermi momentum k_p of the proton. The relation for T_C is given by

$$T_C = T_0\left[\frac{k_p^2}{k_p^2+k_1^2}\right]\left[\frac{(k_p-k_2)^2}{(k_p-k_2)^2+k_3^2}\right], \tag{32}$$

where $k_1 = 1.117$ fm^{-1}, $k_2 = 1.329$ fm^{-1}, $k_3 = 0.1179$ fm^{-1} and $T_0 = 17 \times 10^9 K$. The Fermi momentum k_p is in fm^{-1} units and T_C is non-zero only if $k_p < k_1$. This leads to T_C for the protons peaking somewhat below 10^{10} K, similar to the Λ critical temperature.

Since neutrons are, after all, more abundant than other particles in neutron stars, they have higher energies and at supernuclear densities are unlikely to form $^1S_0$ pairs. They can have a $^3P_2$ pairing as considered in Ref. [49], but it is much weaker and corresponds to a maximum critical temperature $T_C \simeq 3 \times 10^8$ K. Below this temperature the contribution to the critical frequency curve from hyperon bulk viscosity is quite low, most of the contribution coming from viscosity at the crust-core interface. Therefore neutron superfluidity does not much affect the viability of persistent gravitational wave emission from the r-modes, and we neglect it here.

The effect of superfluidity on the microscopic relaxation timescale (15) or (16) appears, after doing the lengthy collision integrals (see HLY and LO), as multiplicative factors in the average matrix elements:

$$\langle|\mathcal{M}_\Sigma|^2\rangle \;\rightarrow\; R_{nnp\Sigma}\langle|\mathcal{M}_\Sigma|^2\rangle, \tag{33}$$

$$\langle|\mathcal{M}_\Lambda|^2\rangle \;\rightarrow\; R_{npp\Lambda}\langle|\mathcal{M}_\Lambda|^2\rangle. \tag{34}$$

If none of the participating particle species is superfluid, an R factor is 1. Each R factor is reduced as more species become superfluid. Our treatment of these factors is based on that used by HLY, who calculate R for the cases when either one or two of the particles participating in the reaction are superfluid. HLY do not however provide a 3-particle R which is required for calculating the timescale of the Λ reaction (13). Our numerical investigations found (III C) that expressing $R_{nnp\Sigma}$ as a product of two single-particle factors $R_p R_{\Sigma^-}$ instead of HLY's two-particle factor does not affect the r-mode critical frequency much. Therefore throughout this paper we express all R's as products of the appropriate single-particle factors. The expression for the single-particle R from Eq. (30) of HLY is

$$R = \frac{a^{5/4} + b^{1/2}}{2} \exp\left(0.5068 - \sqrt{0.5068^2 + y^2}\right), \tag{35}$$

where $y = \Delta(T)/kT$, $a = 1 + 0.3118y^2$ and $b = 1 + 2.566y^2$. LO used a simple factor e^{-y} for the hyperons only, since they were focusing on the ordinary fluid case. The exponential is indeed the dominant behavior of the HLY expression for $y \gg 1$, but the HLY expression is significantly more accurate for y less than about 5–10, which turns out to be the astrophysically interesting region.

We plot the most important results of our microphysics calculations. Figure 2 shows a typical relaxation timescale as a function of density, and Fig. 3 shows the corresponding bulk viscosity coefficient. Among the equations of state we use, H3 has a relaxation timescale in the middle of the distribution. Neglecting superfluidity, the timescales are about a factor of 40 shorter than in LO. About 20 of this comes from making the matrix elements

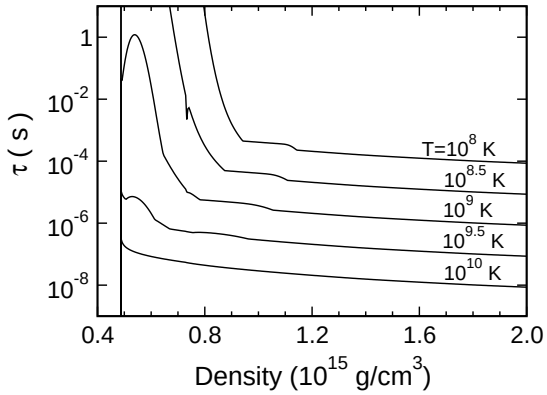

FIG. 2: Microscopic relaxation timescale as a function of density for various temperatures. The equation of state is H3 and the Σ^- and Λ bandgaps are assumed equal. Thus at the highest temperature plotted, no superfluid effects are present.

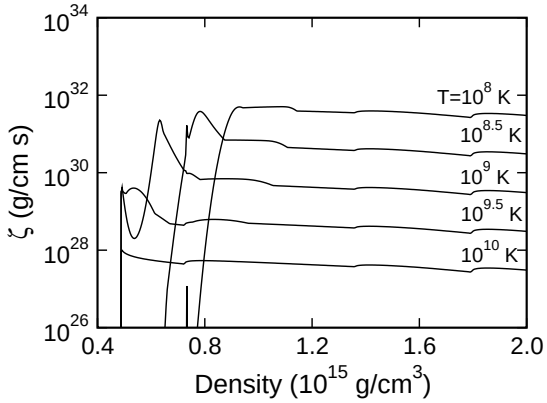

FIG. 3: Bulk viscosity coefficient as a function of density for various temperatures, for the same model as Fig. 2. The star is rotating with angular frequency 2300 radians per second.

consistent with the quasiparticle picture, and most of the rest comes from changes to the equation of state (including accounting for the typos in Ref. [44] which propagated to LO). Fig. 3 is reduced from LO by a further factor of 2 due to the relativistic factor $\gamma_\infty - \gamma_0$. Including superfluidity, the shapes of the curves are different from LO but the peak timescales are comparable. It is difficult to compare to HLY because at these temperatures the high-frequency approximation they use ($\hat{\omega}\tau \gg 1$) does not hold.

III. MACROPHYSICS

With the bulk viscosity coefficient ζ in hand, we can proceed to compute r-mode damping times and critical frequencies. For this we also need the hydrodynamic structure of the r-mode as well as equilibrium models of the structure of a neutron star (i.e. its density profile).

A. Stellar structure

We are motivated by the sensitivity of the hyperon population to the central density to include the effects of general relativity and rotation in our stellar models. Relativistic stellar models have higher densities than non-relativistic ones, and rotating models have lower densities than nonrotating ones. LO used relativistic, non-rotating stellar models; while other work such as HLY and Ref. [21] did not treat the stellar or mode structure in much detail. Since we are interested in exploring a broader parameter space, we do not restrict ourselves to nonrotating stars.

We take into account the effect of rotation on the neutron star structure using Hartle's slow-rotation approximation [50]. Hartle's formalism is based on treating a rotating star as a perturbation on a non-rotating star. We start by solving the Oppenheimer-Volkoff equations for a static spherically symmetric star in a form due to Lindblom [51]

$$\frac{dm}{dh} = -\frac{4\pi\epsilon(h)r(h)^3[r(h)-2m(h)]}{m(h)+4\pi r(h)^3 p(h)}, \quad (36)$$

$$\frac{dr}{dh} = -\frac{r(h)[r(h)-2m(h)]}{m(h)+4\pi r(h)^3 p(h)}, \quad (37)$$

using as independent variable the specific enthalpy

$$h(p) = \int_0^p dp'/[p'+\epsilon(p')]. \quad (38)$$

From $r(h)$, the radius at which the enthalpy is h, and $m(h)$, the mass contained within a sphere of that radius, we find $m(r)$. We also find $\nu(r)$, the logarithm of the time-time metric component which is based on $h(r)$. We then use this solution of the static star to solve for a rotating star with the same central pressure.

The metric of a slowly rotating star to second order in Ω, the spin frequency, can be written as

$$\begin{aligned} ds^2 = & -e^{\nu}\left[1+2(h_0+h_2P_2)\right]dt^2 \\ & + \left[1+\frac{2(m_0+m_2P_2)}{(r-2M(r))}\right]\left[1-\frac{2M(r)}{r}\right]^{-1}dr^2 \\ & + r^2\left[1+2(v_2-h_2)P_2\right]\left[d\theta^2+\sin^2\theta(d\phi-\omega dt)^2\right] \\ & + O(\Omega^3). \end{aligned} \quad (39)$$

Here $P_2 = P_2(\cos\theta)$ is the 2nd order Lagrangian polynomial. The quantity ω is the frame dragging frequency that is proportional to Ω, while h_0, h_2, m_0, m_2, and ν_2 are all functions of r that are proportional to Ω^2. Before we solve the Einstein equations for all the subscripted quantities in Eq. (39) we need to solve for $\bar{\omega} = \Omega - \omega$. This is done by solving

$$\frac{1}{r^4}\frac{d}{dr}\left(r^4 j(r)\frac{d\bar{\omega}(r)}{dr}\right) + \frac{4}{r}\frac{dj(r)}{dr}\bar{\omega}(r) = 0, \quad (40)$$

with the definition

$$j(r) = \exp^{-\nu/2}\left[1-\frac{2M(r)}{r}\right]^{1/2}, \quad (41)$$

and the boundary conditions that at the center of the star $\bar{\omega}(0) = \bar{\omega}_i$, an arbitrary constant, and $(d\bar{\omega}(r)/dr)_{r=0} = 0$. From Eq. (40) one determines Ω and the angular momentum J corresponding to $\bar{\omega}_i$ as follows:

$$J = \frac{1}{6}R^4\left(\frac{d\bar{\omega}(r)}{dr}\right)_{r=R}, \quad (42)$$

$$\Omega = \bar{\omega}(R) + \frac{2J}{R^3}. \quad (43)$$

Here R is the radius of the star. To obtain the desired value of Ω one can scale $\bar{\omega}$ thus:

$$\bar{\omega}(r)_{new} = \bar{\omega}(r)_{old}(\Omega_{new}/\Omega_{old}). \quad (44)$$

The angular momentum J corresponding to Ω_{new} can then be calculated using Eq. (42).

A measure of the change in the star structure caused by rotation is $\xi(r,\theta)$ which represents the displacement of constant energy density surfaces between the rotating star and the corresponding non-rotating star. This displacement's angular dependence can be separated out:

$$\xi(r,\theta) = \xi_0(r) + \xi_2(r)P_2. \quad (45)$$

The $l = 0$ part of this deformation, ξ_0, can be obtained by solving the following equations:

$$\begin{aligned} \frac{dm_0(r)}{dr} = & + 4\pi r^2\frac{d\epsilon(r)}{dp(r)}\left[\epsilon(r)+p(r)\right]p_0^*(r) \\ & + \frac{1}{12}j^2(r)r^4\left(\frac{\bar{\omega}(r)}{dr}\right)^2 \\ & - \frac{1}{3}r^3\frac{dj^2(r)}{dr}\bar{\omega}^2(r), \end{aligned} \quad (46)$$

$$\begin{aligned} \frac{dp_0^*(r)}{dr} = & - \frac{m_0\left[1+8\pi r^2 p(r)\right]^2}{r-2M(r)} \\ & - \frac{4\pi\left[\epsilon(r)+p(r)\right]r^2}{r-2M(r)}p_0^*(r) \\ & + \frac{r^4 j^2(r)}{12\left[r-2M(r)\right]}\left(\frac{d\bar{\omega}(r)}{dr}\right)^2 \\ & + \frac{1}{3}\frac{d}{dr}\left(\frac{r^3 j^2(r)\bar{\omega}^2(r)}{r-2M(r)}\right), \end{aligned} \quad (47)$$

where p_0^* is a pressure perturbation, the density profile $\epsilon(r)$ is the energy density of the non-rotating star as function of r, and $p(r)$ is the pressure of the star as a function of r. The boundary conditions for the above equations are that both m_0 and p_0^* vanish at the origin.

The gravitational mass of the rotating star is given by

$$M'(R) = M(R) + m_0(R) + \frac{J^2}{R^3}, \quad (48)$$

which is greater than the mass of the nonrotating star with the same central pressure. We wish to build sequences of stars rotating at various rates all with the same gravitational mass. To do this we first solve the

Oppenheimer-Volkoff equations; then, solve Eq. (40), (46), and (47); then calculate the new mass of the rotating star using Eq. (48). This procedure is repeated with lower values of the central pressure until the same mass as the nonrotating star is obtained.

To perform the viscosity calculations we need information on the structure of the rotating star contained in its density profile. Once the correct mass is obtained the density profile $\epsilon(r)$ is calculated by using

$$\epsilon_{rot}(r) = \epsilon_{stat}(r) - \frac{d\epsilon_{stat}(r)}{dr}\xi_0(r), \tag{49}$$

where

$$\xi_0(r) = -p_0^*(r)\frac{\epsilon(r)+p(r)}{dp(r)/dr}. \tag{50}$$

Here, $\epsilon_{rot}(r)$ is the density profile of the rotating star, while $\epsilon_{stat}(r)$ is the density profile of the non-rotating one. This yields only the spherically symmetric part of the density perturbation, which is the dominant one for our purposes.

B. Driving and damping timescales

The stability of an r-mode is determined by calculating the damping and driving timescales. The mode is unstable if the driving timescale is shorter than the viscous damping timescale. This can be expressed in terms of an overall r-mode timescale τ_r such that

$$\frac{1}{\tau_r(\Omega,T)} = \frac{1}{\tau_{GR}(\Omega)} + \frac{1}{\tau_V(\Omega,T)}, \tag{51}$$

where $\tau_{GR} < 0$ is the damping timescale of the mode due to gravitational radiation and $\tau_V > 0$ is the damping timescale resulting from the sum of all viscous processes in the star. The star's spin angular frequency and temperature are represented by Ω and T, respectively. A mode unstable to gravitational radiation corresponds to $\tau_r < 0$ in Eq. (51), and the critical frequency Ω_c of the star as a function of temperature is found by solving $1/\tau_r(\Omega_c, T) = 0$.

The gravitational radiation timescale is given by

$$\frac{1}{\tau_{GR}} = -\frac{1}{2\tilde{E}}\left(\frac{d\tilde{E}}{dt}\right)_{GR}, \tag{52}$$

where $\tilde{E}$ is the mode energy in a frame rotating with the star and $(d\tilde{E}/dt)_{GR}$ is the rate at which energy is emitted in gravitational waves in the same frame. For the current quadrupole r-mode, there exist simple expressions (to lowest order in mode amplitude and angular velocity of the star) for the energy and gravitational radiation timescale: [30]

$$\begin{aligned}\tilde{E} &= \frac{1}{2}\alpha^2\Omega^2 R^{-2}\int_0^R \epsilon(r) r^6 dr,\\ \frac{1}{\tau_{GR}} &= -\frac{131\,072\pi}{164\,025}\int_0^R \epsilon(r) r^6\, dr.\end{aligned} \tag{53}$$

Here α is a dimensionless amplitude coefficient which cancels out of the driving and damping timescales.

The viscous damping time scale τ_V is given by

$$\frac{1}{\tau_V} = -\frac{1}{2\tilde{E}}\left(\frac{d\tilde{E}}{dt}\right)_V, \tag{54}$$

where $(d\tilde{E}/dt)_V$ is the rate at which energy is being drained from the mode by viscosity. Here we consider only hyperon bulk viscosity from the nonleptonic processes discussed in the previous section. Leptonic (Urca) processes also contribute, but in LO they were shown to be overwhelmed by the viscosity due to nonleptonic processes. Although the crust-core viscosity is important at low temperatures—it determines the shape of the negatively sloped part of the instability curve which in turn puts a constraint on how much farther along the temperature axis the rising part of the instability curve should be located at to prevent a thermal runaway—we neglect it. For a reasonable estimate of the shape of the crust-core viscosity curve and of the value of the saturation amplitude the stars temperatures hould increase to around 10^9 K [31]. To explore the effect of the crust-core viscosity and the saturation amplitude in more details is beyond the scope of this paper. We can then compute the viscous damping timescale as in LO: To lowest order in Ω, we can write

$$\left(\frac{d\tilde{E}}{dt}\right)_V = -4\pi\int_0^R \zeta(\epsilon(r))\langle|\vec{\nabla}\cdot\delta\vec{v}|^2\rangle r^2\, dr, \tag{55}$$

where $\langle|\vec{\nabla}\cdot\delta\vec{v}|^2\rangle$ is the angle average of the square of the hydrodynamic expansion. LO found that the expansion found numerically in Ref. [52] could be fit well by

$$\langle|\vec{\nabla}\cdot\delta\vec{v}|^2\rangle = \frac{\alpha^2\Omega^2}{690}\left(\frac{r}{R}\right)^6\left[1+0.86\left(\frac{r}{R}\right)^2\right]\left(\frac{\Omega^2}{\pi G\bar{\epsilon}}\right)^2, \tag{56}$$

where $\bar{\epsilon}$ is the mean density of the (nonrotating) star. [In Eq. (6.6) of LO the last factor is missing due to a misprint, but is properly included in the calculations.] This approximation breaks down for $r/R \approx 1$, but since the bulk viscosity is coming from the hyperon core that is enough. In Table II we give typical radii of nonrotating stars and their hyperon cores.

C. Critical frequency curves

We are now in a position to solve for the critical frequency as a function of temperature for various neutron star models. This must be done numerically.

Because of the inclusion of rotation the process is somewhat more involved than in LO. The critical frequency curve is calculated in two stages to ensure that the correct gravitational mass is retained after including the corrections to it from rotation. In the first stage we calculate

EOS	ϵ_c (10^{14}g/cm^3)	R (km)	R_Σ (km)	R_Λ (km)
H3	6.86	13.74	6.38	0.00
H4	6.12	13.85	4.50	0.00
H5	7.70	13.33	5.37	0.00
H6	7.84	13.44	6.70	2.46
H7	9.00	13.01	6.03	0.00

TABLE II: Parameters of non-rotating $1.4M_\odot$ equilibrium stars for each equation of state (EOS). The central mass density is ϵ_c, R is the stellar radius, R_Σ is the distance out to which Σ^- hyperons appear, and R_Λ is the corresponding distance for Λ hyperons.

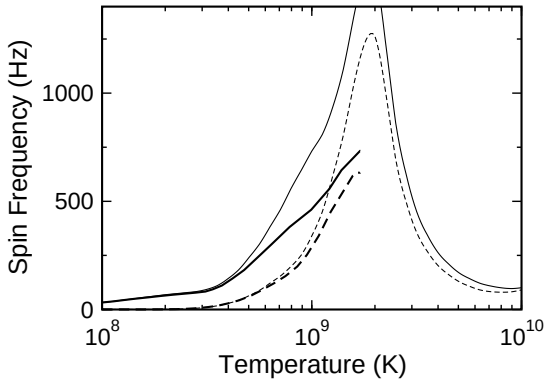

FIG. 4: Critical frequency curves $1.4M_\odot$ neutron stars with equal bandgaps for Σ^- and Λ hyperons. The dashed curve is for equation of state H3 and the solid curve is for H6. The thinner curves neglect the effect of rotation on stellar structure while the thicker curves include it. The curves including rotation are extended to their peaks, but no further.

the critical frequency as a function of temperature for a nonrotating star using the Oppenheimer-Volkoff formalism. Then a set of points on this curve is taken. In the second stage, for each point we find the structure (density profile) of a star rotating at that frequency with the same gravitational mass as the nonrotating star. Since Hartle's formalism produces stars with greater gravitational masses, this step requires several iterative trials of the central pressure to find the star with the same gravitational mass. Using the new density profile with rotation, we keep the frequency fixed and use the corresponding temperature on the nonrotating curve as an initial guess for a routine that finds the root of $1/\tau_r$, thereby obtaining the correct temperature for the marginally star rotating at that frequency. Because of this it is cumbersome to trace out parts of the curves where the critical frequency decreases with temperature, and since those parts of the bulk viscosity curves are not important for determining the viability of persistent gravitational wave emission we neglect them.

The importance of rotation is shown in the critical frequency curves plotted in Fig. 4. (Kepler frequencies for these equations of state are 750–850 Hz for 1.4 $M_\odot$ stars.) Equation of state H6 is soft and has the highest hyperon population for a given mass, and thus its curve is higher than for H3 which is intermediate. This plot shows the general trend that the effect of rotation is more significant for softer equations of state. For persistent gravitational wave emission the key question is whether or not a neutron star undergoing thermal runaway will be blocked by hitting the curve at a temperature lower than a few times 10^9 K. Even for the soft H6 equation of state, the effect of rotation on stellar structure changes the temperature at which a star hits the curve by no more than a factor of 2 (still within the region that is good for gravitational wave emission). More significant is the fact that the frequency at which the curve peaks can be considerably reduced from the value neglecting rotation. If the peak is low enough, thermal runaway can still occur—for example in this plot it can occur for H3 stars if they hit above 700 Hz—and the outlook is bad for persistent gravitational wave emission.

In Fig. 5 we show the effect of the equation of state on the critical frequency curve for 1.4 $M_\odot$ stars. The curves generically reach their peak at temperatures of 1–2×10^9 K, which is good for persistent gravitational wave emission. However, the heights (frequencies) of the peaks change significantly. The peak is highest for H6, which has the largest hyperon population. It is almost identical for H3 and H7, although those two equations of state are the furthest separated in the (K, m^*, x_σ) parameter space. This seems to be due to the similar radii of their hyperon-containing cores as in Table II. All three of these equations of state then allow persistent gravitational wave emission in 1.4 $M_\odot$ stars. The peak is lowest for H4, which is not surprising since that is the stiffest equation of state and has the lowest hyperon population. For H4 the peak is so low that, depending on the details of the crust-related damping, the full curve including that damping might show no significant effect from hyperon bulk viscosity—it might decrease throughout the temperature range and never allow persistent emission. In any case, for H4 and H5 persistent emission is not possible for the most rapidly rotating stars in LMXBs (up to 619 Hz) if they are 1.4 $M_\odot$. This demonstrates in principle how observation of r-mode gravitational waves from an LMXB could rule out some equations of state or, more broadly, constrain hyperon populations.

In Fig. 6 we plot critical frequency curves for stars with different masses for the H4 equation of state, which is the stiffest of those we use. (For other equations of state, the stellar mass affects the curve more but is constrained to a narrower range, so the overall variation is greatest for H4.) We also vary the Σ^- bandgap from the Λ value to 10 times that value. It can be seen that increasing the mass pushes the curve to lower temperatures and raises its peak. This is due to the fact that higher mass stars have higher central densities and hence, in absolute terms, larger hyperon populations than their lower mass counterparts. Persistent r-mode gravitational wave emission is viable in all but the 1.4 $M_\odot$ neutron stars.

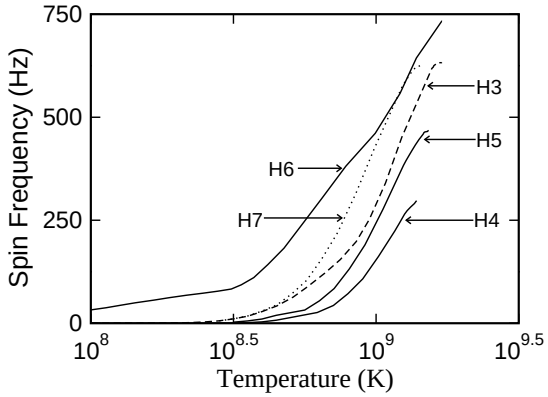

FIG. 5: Critical frequency as a function of temperature for 1.4 $M_\odot$ stars with different equations of state. All curves assume the superfluid bandgaps of the Λ and Σ^- hyperons are equal.

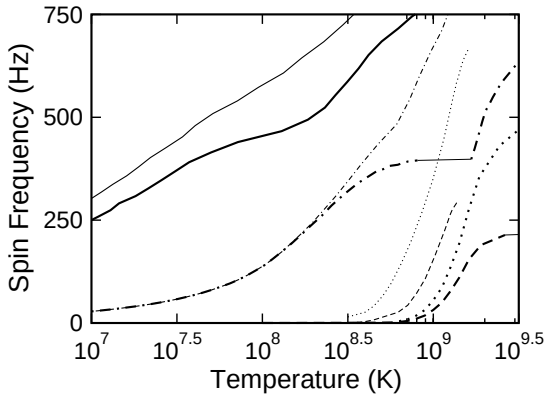

FIG. 6: Instability curves for H4 stars with different masses. The thicker curves use the larger Σ^- bandgap while the thinner curves use the smaller one. The solid lines represent $2.0M_\odot$ stars, the dot-dash lines repsents $1.8M_\odot$ stars, the dotted line represents $1.6M_\odot$ stars, and the dashed line represents $1.4M_\odot$ stars.

The temperature at which this can happen is strongly dependent on the mass, and to a lesser but still significant extent (factor 3) on the Σ^- bandgap, with higher bandgaps leading to higher temperatures at a given frequency. (The small horizontal sections of the $1.4M_\odot$ and $1.6M_\odot$ large bandgap curves should actually dip slightly. This behavior is missed due to our method of including rotation, but is unimportant for the thermal runaway and persistent gravitational wave emission.)

The curves for 1.8–2.0 $M_\odot$ stars are particularly interesting in light of predicted interior temperatures of neutron stars in LMXBs. These can be determined from observations in quiescence of the surface temperatures of three slowly accreting neutron stars mentioned in Brown, Bildsten, and Chang [53]. To calculate the interior temperatures we use Fig. 2 from Yakovlev et al [54], which depicts the relationship between the core and the measured surface temperatures using different atmospheric

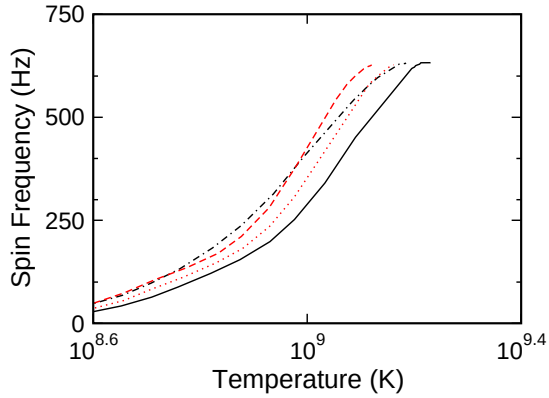

FIG. 7: Variations on the critical frequency curve for a 1.4 $M_\odot$ H3 star with equal Λ and Σ^- bandgaps. The solid curve is our standard model. The dotted curve uses asymptotic values for the axial couplings instead of vacuum at-rest values. The dot-dash curve uses the 2-particle superfluid reduction factor for the Σ^- interaction instead of two 1-particle factors. The dashed curve simulates the fast timescales predicted by van Dalen and Dieperink.

and equation of state models. We thereby obtain a temperature range (1.5×10^7–4×10^8K) which covers LMXBs whose thermal emission spectra have been observed. This result is probably statistically biased, since LMXBs with higher accretion rates are likely to have higher temperatures but surface temperatures are harder to observe because of the accretion discs. At any rate, the most massive H4 stars have critical frequency curves which would allow gravitational wave emission scenarios [34, 35] to operate in that temperature range. Less massive stars allow it at higher temperatures, which may be consistent with the more rapidly accreting neutron stars such as Sco X-1 whose temperatures are poorly known.

The effects of varying some additional microphysical parameters are shown in Fig. 7, which depicts curves for 1.4 $M_\odot$ neutron stars with the H3 equation of state and the Σ^- superfluidity bandgap equal to that of the Λ. The variations include using the asymptotic (quark) values for the axial-vector couplings in the reaction rates, using HLY's two-particle superfluid reduction factor instead of the product of two one-particle factors, and using relaxation times an order of magnitude faster from van Dalen and Dieperink [21]. All of these curves peak at almost identical frequencies, and the temperature at a fixed frequency changes by less than a factor of 1.5 Therefore, the changes to these microphysical parametrs do not affect our earlier conclusions. From an astrophysical point of view, the most sensitive unknowns in this complicated calculation are the hyperon population (thus the equation of state and stellar mass) and superfluid bandgaps. At a very simple level this makes sense because the hyperons appear only after a threshold density and the bandgaps appear in exponential factors rather than power laws.

IV. DISCUSSION

We have extended previous investigations of r-modes in accreting hyperon stars in LMXBs as persistent sources of gravitational waves, focusing on the bulk viscosity which is needed to prevent thermal runaway. We have used improved microphysics compared to previous treatments, and have accounted for the most important macroscopic correction due to rotation of the star.

We find that persistent gravitational wave emission is quite robust. Even the stiffest hyperonic equations of state in relativistic mean field theory produce enough damping to stop the runaway and persistently radiate, although some of them require neutron stars somewhat more massive than 1.4 $M_\odot$. Stars below about 1.3 $M_\odot$ are not likely to be persistent sources regardless of the equation of state. The mass thresholds are somewhat more favorable for lower superfluid bandgaps than for higher bandgaps. Other details of the microphysics are found to be considerably less important. Our results seem robust for typical values of the crust-core viscosity and of saturation amplitude of r-modes, though this issue requires further investigation. Stars with high masses and stiff equations of state could exist in thermal and torque equilibrium at temperatures down to 10^7 K.

One possible avenue for substantial improvement is the hydrodynamics. We used a fluid expansion in the dissipation integrals which is a reasonable approximation for a Newtonian normal fluid, but not for a superfluid which can be much more complicated due to multiple components and entrainment. Work is underway to deal with the superfluid problem in general ([55] and references therein).

Acknowledgments

This work was supported by the National Science Foundation under grants PHY-0245649 and PHY-0114375 (the Penn State Center for Gravitational Wave Physics). We are especially grateful to Lee Lindblom for many helpful discussions, including confirming errors in previous work. We also thank Lars Bildsten, Ian Jones and Dimitri Yakovlev for helpful discussions.

[1] N. Stergioulas, Living Rev. Rel. **6**, 3 (2003), and references therein, gr-qc/0302034.
[2] B. J. Owen et al., Phys. Rev. **D58**, 084020 (1998), gr-qc/9804044.
[3] L. Bildsten, Astrophys. J. **501**, L89 (1998), astro-ph/9804325.
[4] N. Andersson, K. D. Kokkotas, and N. Stergioulas, Astrophys. J. **516**, 307 (1999), astro-ph/9806089.
[5] J. Papaloizou and J. Pringle, Mon. Not. R. Astron. Soc. **184**, 501 (1978).
[6] R. V. Wagoner, Astrophys. J. **278**, 345 (1984).
[7] A. K. Schenk, P. Arras, E. E. Flanagan, S. A. Teukolsky, and I. Wasserman, Phys. Rev. **D65**, 024001 (2002), gr-qc/0101092.
[8] S. M. Morsink, Astrophys. J. **571**, 435 (2002), astro-ph/0202051.
[9] P. Arras et al., Astrophys. J. **591**, 1129 (2003), astro-ph/0202345.
[10] J. Brink, S. A. Teukolsky, and I. Wasserman, Phys. Rev. **D70**, 121501 (2004), gr-qc/0406085.
[11] J. Brink, S. A. Teukolsky, and I. Wasserman, Phys. Rev. **D70**, 124017 (2004), gr-qc/0409048.
[12] J. Brink, S. A. Teukolsky, and I. Wasserman, Phys. Rev. **D71**, 064029 (2005), gr-qc/0410072.
[13] P. M. Sa and B. Tome, Phys. Rev. **D71**, 044007 (2005), gr-qc/0411072.
[14] W. D. Langer and A. G. W. Cameron, Astrophys. Space Sci. **5**, 213 (1969).
[15] P. B. Jones, Astrophys. Lett. **5**, 33 (1970).
[16] P. B. Jones, Proc. Roy. Soc. (London) **A323**, 111 (1971).
[17] P. B. Jones, Phys. Rev. Lett. **86**, 1384 (2001).
[18] P. B. Jones, Phys. Rev. **D64**, 084003 (2001).
[19] L. Lindblom and B. J. Owen, Phys. Rev. **D65**, 063006 (2002), astro-ph/0110558.
[20] P. Haensel, K. P. Levenfish, and D. G. Yakovlev, Astron. Astrophys. **381**, 1080 (2002), astro-ph/0110575.
[21] E. N. E. van Dalen and A. E. L. Dieperink, Phys. Rev. **C69**, 025802 (2004), nucl-th/0311103.
[22] J. Madsen, Phys. Rev. Lett. **81**, 3311 (1998), astro-ph/9806032.
[23] L. Lindblom, B. J. Owen, and G. Ushomirsky, Phys. Rev. **D62**, 084030 (2000), astro-ph/0006242.
[24] Y. Levin and G. Ushomirsky, Mon. Not. Roy. Astron. Soc. **324**, 917 (2001), astro-ph/0006028.
[25] Y. Wu, C. D. Matzner, and P. Arras, Astrophys. J. **549**, 1011 (2001), astro-ph/0006123.
[26] J. B. Kinney and G. Mendell, Phys. Rev. **D67**, 024032 (2003), gr-qc/0206001.
[27] D. Chakrabarty et al., Nature **424**, 42 (2003), astro-ph/0307029.
[28] Y. Levin, Astrophys. J. **517**, 328 (1999), astro-ph/9810471.
[29] H. C. Spruit, Astron. Astrophys. **341**, L1 (1999), astro-ph/9811007.
[30] L. Lindblom, B. J. Owen, and S. M. Morsink, Phys. Rev. Lett. **80**, 4843 (1998), gr-qc/9803053.
[31] J. S. Heyl, Astrophys. J. **574**, L57 (2002).
[32] C. Cutler and K. S. Thorne (2002), gr-qc/0204090.
[33] R. V. Wagoner, J. F. Hennawi, and J.-s. Liu (2001), astro-ph/0107229.
[34] A. Reisenegger and A. A. Bonacic, Phys. Rev. Lett. **91**, 201103 (2003), astro-ph/0303375.
[35] R. V. Wagoner, Astrophys. J. **578**, L63 (2002), astro-ph/0207589.
[36] R. V. Wagoner, AIP Conf. Proc. **714**, 224 (2004), astro-ph/0312433.
[37] N. Andersson, D. I. Jones, and K. D. Kokkotas, Mon. Not. Roy. Astron. Soc. **337**, 1224 (2002), astro-ph/0111582.
[38] N. K. Glendenning, *Compact Stars: Nuclear Physics,*

Particle Physics, and General Relativity (Springer, New York, 2000), 2nd ed.
[39] B. D. Lackey, M. Nayyar, and B. J. Owen, Phys. Rev. **D73**, 024021 (2006), astro-ph/0507312.
[40] D. G. Yakovlev and C. J. Pethick, Ann. Rev. Astron. Astrophys. **42**, 169 (2004), astro-ph/0402143.
[41] D. J. Nice et al., Astrophys. J. **634**, 1242 (2005), astro-ph/0508050.
[42] S. M. Ransom et al., Science **307**, 892 (2005), astro-ph/0501230.
[43] J. Cottam, F. Paerels, and M. Mendez, Nature **420**, 51 (2002), astro-ph/0211126.
[44] N. K. Glendenning, Astrophys. J. **293**, 470 (1985).
[45] K. Hagiwara et al. (Particle Data Group), Phys. Rev. **D66**, 010001 (2002).
[46] N. W. Ashcroft and N. D. Mermin, *Solid State Physics* (Brookes Cole, 1976), 1st ed.
[47] S. Balberg and N. Barnea, Phys. Rev. **C57**, 409 (1998), nucl-th/9709013.
[48] T. Takatsuka, S. Nishizaki, Y. Yamamoto, and R. Tamagaki, Prog. Theor. Phys. **105**, 179 (2001).
[49] A. D. Kaminker, D. G. Yakovlev, and O. Y. Gnedin, Astron. Astrophys. **383**, 1076 (2002).
[50] J. B. Hartle, Astrophys. J. **150**, 1005 (1967).
[51] L. Lindblom, Astrophys. J. **398**, 569 (1992).
[52] L. Lindblom, G. Mendell, and B. J. Owen, Phys. Rev. **D60**, 064006 (1999), gr-qc/9902052.
[53] E. F. Brown, L. Bildsten, and P. Chang, Astrophys. J. **574**, 920 (2002), astro-ph/0204102.
[54] D. G. Yakovlev, K. P. Levenfish, A. Y. Potekhin, O. Y. Gnedin, and G. Chabrier, Astron. Astrophys. **417**, 169 (2004), astro-ph/0310259.
[55] N. Andersson and G. L. Comer (2005), physics/0509241.